

# Strain-Release Assembly of Nanowires on Stretchable Substrates

Feng Xu,<sup>†</sup> John W. Durham, III,<sup>†</sup> Benjamin J. Wiley,<sup>‡</sup> and Yong Zhu<sup>†,\*</sup>

<sup>†</sup>Department of Mechanical and Aerospace Engineering, North Carolina State University, Raleigh, North Carolina 27695, United States, and <sup>‡</sup>Department of Chemistry, Duke University, Durham, North Carolina 27708, United States

Over the past decade, both semiconductor and metallic nanowires (NWs) have been actively explored as building blocks for next-generation electronics, optoelectronics, and sensors,<sup>1–3</sup> including flexible and transparent devices<sup>4–8</sup> as well as stretchable devices.<sup>9</sup> A critical step in constructing NW-based devices is assembly (including transfer, alignment and density control) of NWs on a substrate for device fabrication. Scalable and controlled assembly of NWs synthesized with diverse methods (*e.g.*, wet or dry methods) on diverse substrates (*e.g.*, silicon, plastics, and rubbers) presents a major fabrication challenge that must be overcome if NWs are to be utilized in practical applications. Methods for controlling the assembly and alignment of NWs include those that utilize electrical-fields,<sup>10,11</sup> Langmuir–Blodgett troughs,<sup>12,13</sup> microfluidics,<sup>14,15</sup> blown-bubble-films,<sup>16,17</sup> “knocking-down” motion,<sup>18</sup> and contact printing.<sup>19–21</sup> While significant progress has been made,<sup>22</sup> large-scale assembly of NWs still remains a challenging task.

In this paper, we present a simple strategy for NW assembly. The NWs were assembled on top of elastomeric substrates; when a strained substrate was released, the NWs aligned in the transverse direction and the area coverage of the NWs on the substrate increased. We find that the large-strain elasticity of the substrates and the static friction between the NWs and the substrates play key roles in the NW alignment. This method can be applied to NWs synthesized by different methods or processed in different conditions (*e.g.*, wet or dry methods). In addition, it can be combined with the other reported methods to improve the alignment. Controlled assembly of silver (Ag) and silicon (Si) NWs on poly(dimethylsiloxane) (PDMS) substrates were demonstrated. This paper starts with an analysis of NW motion in response to the

**ABSTRACT** A simple yet effective method for assembly of highly aligned nanowires (NWs) on stretchable substrates is reported. In this method, NWs were first transferred to a strained stretchable substrate. After the strain was released, the NWs aligned in the transverse direction and the area coverage of the NWs on the substrate increased. This method can be applied to any NWs deposited on a stretchable film and can be repeated multiple times to increase the alignment and density of the NWs. For silver (Ag) and silicon (Si) NWs on poly(dimethylsiloxane) (PDMS) substrates, the probability of NW alignment increased from 29% to 90% for Ag NWs, and from 25% to 88% for Si NWs after two assembly steps; the density increased by 60% and 75% for the Ag and Si NWs, respectively. The large-strain elasticity of the substrate and the static friction between the NWs and the substrate play key roles in this assembly method. We find that a model that takes into account the volume incompressibility of PDMS reliably predicts the degree of NW alignment and NW density. The utility of this assembly method was demonstrated by fabricating a strain sensor array composed of aligned Si NWs on a PDMS substrate, with a device yield of 95%.

**KEYWORDS:** nanowire · assembly · alignment · strain · static friction

release of a strained substrate, followed by demonstrations of controlled assembly with Ag and Si NWs.

## RESULTS AND DISCUSSION

Figure 1 shows schematically how a NW on strained PDMS moves when the PDMS is released. The NW motion is due to the geometric compatibility with the PDMS and the static friction between them. It is well-known that PDMS is an elastomeric material that can undergo large, nonlinear elastic deformation. For a NW with initial length  $L_0$  and skew angle  $\theta_0$ , the width, height, and area of the rectangle bounding the NW are  $L_0 \sin \theta_0$ ,  $L_0 \cos \theta_0$  and  $A_0 = L_0^2 \sin \theta_0 \cos \theta_0$ , respectively (Figure 1a). When the strain is released, assuming linear elasticity, the width, height, and area of the rectangle change to  $L_0 \sin \theta_0 / (1 + \epsilon_{\text{pre}})$ ,  $L_0 \cos \theta_0 / (1 + \nu \epsilon_{\text{pre}})$  and  $A_1 = A_0 / ((1 + \epsilon_{\text{pre}})(1 - \nu \epsilon_{\text{pre}}))$ , respectively, where  $\epsilon_{\text{pre}}$  is the strain and  $\nu$  is the Poisson's ratio. Note that the Poisson's ratio is defined in the linear elasticity model, which is only valid for a small deformation. The Poisson's ratio of PDMS is approximately 0.5.

\*Address correspondence to yong\_zhu@ncsu.edu.

Received for review November 23, 2010 and accepted January 13, 2011.

Published online February 02, 2011  
10.1021/nn103183d

© 2011 American Chemical Society

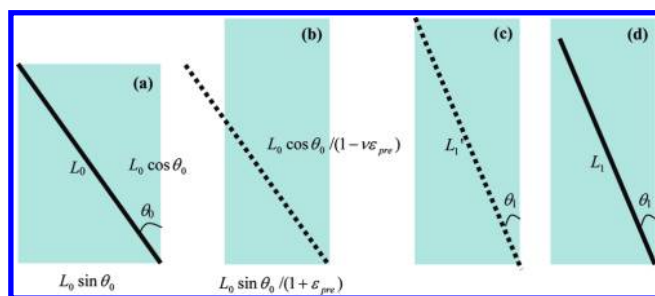


**Figure 1.** Schematics showing the mechanism of NW alignment: (a) a NW transferred to a strained PDMS with a rectangle of PDMS bounding the NW; (b) a virtual NW after release of the strained PDMS, assuming no static friction between the NW and the PDMS; (c) a virtual NW after release of the strained PDMS, assuming a large static friction between the NW and the PDMS; (d) the real NW after release of the strained PDMS.

In the case of no static friction (*i.e.*, no bonding) between the NW and the PDMS, the NW would not move at all (Figure 1b). In the case of static friction (*i.e.*, no sliding) between the NW and the PDMS (Figure 1c), the new NW length and skew angle are  $L_1' = ([\sin \theta_0 / (1 + \epsilon_{pre})]^2 + [\cos \theta_0 / (1 - \nu \epsilon_{pre})]^2)^{1/2} L_0$  and  $\theta_1 = \arctan(((1 - \nu \epsilon_{pre}) \tan \theta_0) / (1 + \epsilon_{pre}))$ , respectively. The length ratio ( $L_1'/L_0$ ) and the new skew angle are plotted in Figure 2 panels a and b as functions of the strain and the initial skew angle. The NW density is inversely proportional to the associated area (*i.e.*, the total number of NWs is equal to the NW density times the area). The density increase is given by  $((1/A_1) - (1/A_0)) / (1/A_0) = (1 - \nu) \epsilon_{pre} - \nu \epsilon_{pre}^2$  and plotted in Figure 2c as a function of the strain.

If the strain involved in the alignment process is very large, the linear elastic treatment of the substrate becomes inaccurate. Instead the nonlinear elasticity should be used,<sup>23</sup> where a term called stretch ( $\lambda$ ) is used in place of strain ( $\lambda = 1 + \epsilon_{pre}$ ). A key assumption in the nonlinear elasticity of elastomeric materials is that the volume does not change during the deformation; in other words, when the material is stretched by  $\lambda$  (or  $1/\lambda$ ) in the axial direction, it shrinks by  $\lambda^{-1/2}$  (or  $\lambda^{1/2}$ ) in the two transverse directions. In our case, the length, height, and area of the rectangle change to  $(L_0 \sin \theta_0) / \lambda$ ,  $(L_0 \cos \theta_0) \lambda^{1/2}$ , and  $A_1 = A_0 \lambda^{-1/2}$ , respectively. The new NW length and skew angle are  $L_1' = ([\sin \theta_0 / \lambda]^2 + [\cos \theta_0 \lambda^{1/2}]^2)^{1/2} L_0$  and  $\theta_1 = \arctan(\lambda^{-3/2} \tan \theta_0)$ , respectively. The density increase is given by  $\lambda^{1/2} - 1$ .

It can be seen in Figure 2 that the formulas for the linear elasticity and nonlinear elasticity give rise to similar results at a small strain, but differ significantly at a large strain. As shown in the Supporting Information and the NW alignment experiments, the formula for nonlinear elasticity predicts the degree of NW alignment and density increase in the experimental results, while the assumption of linear elasticity overestimates alignment but underestimates density. The largest strain used in our analysis was 160%, the reported fracture strain of PDMS.<sup>24</sup> It can be seen from Figure 2 panels b and c that a larger strain leads to better alignment and higher density of NWs.

If the static friction is large, the NW could be stretched or compressed depending on the (substrate) strain and initial skew angle, as shown in Figure 2a. With the assumption of a uniformly distributed static friction, the axial stress on the NW due to the static friction is given by

$$\sigma(x) = \frac{\tau wx}{A} \quad (1)$$

where  $\tau$  is the shear strength (static friction per unit area),  $w$  is the contact width between the NW and the substrate,  $x$  is the Euler coordinate ranging from 0 to  $L_0$ , and  $A$  is the NW cross-sectional area. The total length change of the NW is

$$\Delta L = \int_0^{L_0} \frac{\sigma(x)}{E} dx = \int_0^{L_0} \frac{\tau wx}{EA} dx = \frac{\tau w L_0^2}{2EA} \quad (2)$$

where  $E$  is the Young's modulus of the NW. The average axial strain of the NW is

$$\bar{\epsilon} = \frac{\Delta L_0}{L_0} = \frac{\tau w L_0}{2EA} \quad (3)$$

For a typical hexagonal Si NW with a length of  $10 \mu\text{m}$ , a diameter of 40 nm (contact width is 20 nm) and a Young's modulus of 187 GPa,<sup>25</sup> a shear strength of 19.3 MPa is required in order to accomplish an axial strain (either tension or compression) of 1%. The real static friction is too small to accommodate this strain. The shear strengths of InAs NW on both silicon oxide and silicon nitride substrates ranged from 0.1 to 5 MPa.<sup>26,27</sup> Various nanostructure/substrate systems also gave rise to shear strengths of 0.1–1 MPa.<sup>28–30</sup> Our recent work found that the shear strength between Si NW and PDMS ranged from 0.08 to 6.05 MPa depending on the ultraviolet/ozone (UVO) treatment of PDMS. Details on the study of static friction will be reported elsewhere.<sup>31</sup> As the static friction is not large enough to hold the axial strain as predicted in Figure 2a, we conclude the NW slides on top of the PDMS, giving rise to a negligible axial strain (Figure 1d). On the other hand, if the tensile or compressive strain in the NWs is desired (*e.g.*, to tailor their electrical or optical properties),<sup>32</sup> the above analysis

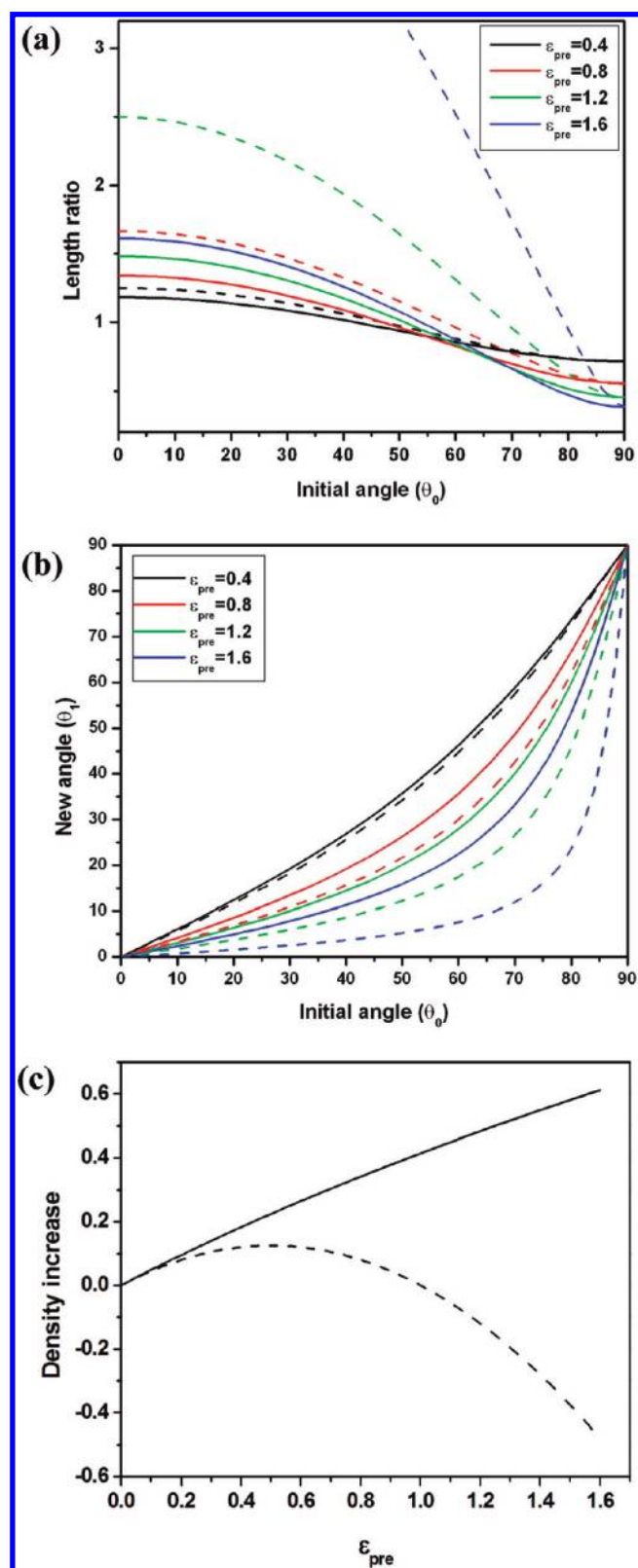


Figure 2. (a) The length ratio ( $L_1/L_0$ ) (assuming a large static friction between NWs and PDMS) and (b) the new skew angle ( $\theta_1$ ) as functions of the strain and initial skew angle. (c) The density increase as a function of the strain. In panels a–c, the dash lines represent the linear elastic analysis and the solid lines represent the nonlinear elastic analysis.

suggests this can be achieved by modifying the surfaces of the NWs or the PDMS in order to increase the static friction between them.

To demonstrate the general applicability of the proposed alignment method,  $\text{Ag}^{33}$  and  $\text{Si}^{25,34}$  NWs were selected as two model materials to represent

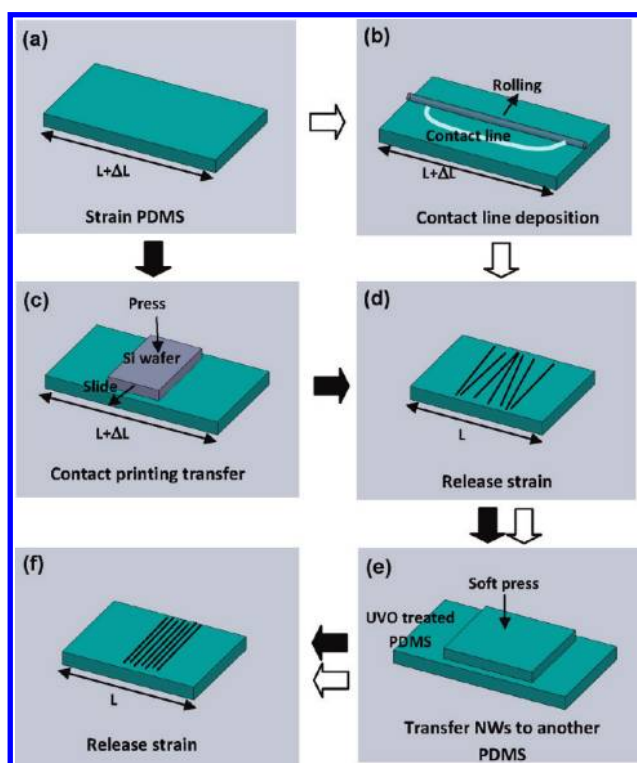


Figure 3. Schematic illustration showing the process of NW assembly. (a) PDMS was mechanically stretched to a desired level of strain. (b) Ag NWs were deposited by the contact line deposition. (c) Si NWs were deposited by the contact printing method. (d) The strain of the PDMS substrate was released. (e) The NWs were transferred from the first PDMS to the second (strained) PDMS substrate to further increase alignment and density. (f) The strain of the second substrate was released.

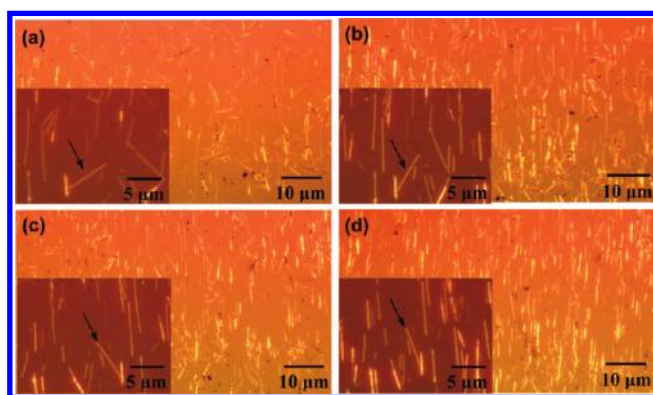
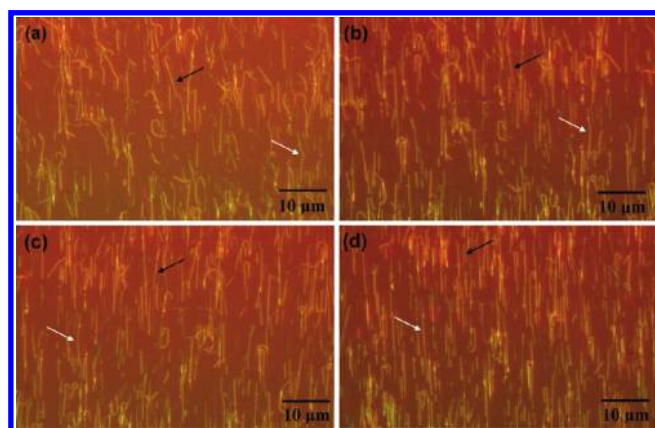


Figure 4. Optical images showing the alignment process of Ag NWs (a) after the contact-line deposition and (b) after the strain on the PDMS substrate was released. (c and d) Images before and after strain release of the second PDMS substrate.

NWs grown in solution or on a substrate, respectively. Figure 3 is a schematic illustration showing the process of the alignment method. A mechanical testing stage (Ernest F. Fullam) was used to mechanically stretch the PDMS substrate to a desired level of strain, as shown in Figure 3a. Then, two different strategies based on contact line deposition<sup>35</sup> and contact printing<sup>19</sup> were adopted to transfer Ag and Si NWs, respectively, to the PDMS substrate. For Ag NWs, the NW solution was first dropped on the strained PDMS substrate, and a glass tube was brought into contact with the drop and the PDMS substrate. A contact line formed between the solvent and the substrate (Figure 3b); the capillary flow

sorted the NWs along the contact line during the rolling process.<sup>35</sup> Gradually rolling the tube moved the contact line across the PDMS substrate, and the NWs deposited along the contact line. As a result, a roughly aligned film of Ag NWs was obtained. For Si NWs, the growth substrate was placed upside down on top of the strained PDMS substrate. A gentle downward pressure was applied on the growth substrate, and it was moved perpendicular to the stretching direction (Figure 3c).<sup>19</sup> After the growth substrate was removed, the PDMS was coated with a roughly aligned film of Si NWs. For both the contact printing and contact line deposition techniques, when the



**Figure 5.** Optical images showing the alignment process of Si NWs (a) after contact printing and (b) after the strain on the PDMS substrate was released. (c and d) Images before and after strain release of the second PDMS substrate. The white arrows indicate how the curved NWs were straightened, and the black arrows indicate how the skewed NWs were aligned.

PDMS substrate was released, the alignment and density of the NWs increased (Figure 3d).

Subsequent transfers of the NWs can be performed to further increase the alignment and density. Adhesion between NWs and PDMS is critical to the yield of NW transfer. To increase the adhesion, subsequent PDMS substrates were radiated under a UV lamp (BHK, Inc.) for  $\sim 5$  min with the assistance of UV-generated ozone.<sup>36–38</sup> As shown in Figure 3e, the first (released) PDMS sheet with NWs was then brought into contact with the second (strained) one that had been treated by UVO. After a short contact (*e.g.*, a few minutes), the first PDMS was slowly peeled from the second one, and the NW film was left on the second PDMS substrate. Releasing the strain of the second PDMS substrate further increased the NW alignment and density (Figure 3f). These transfer/release steps can be repeated multiple times as needed to further improve NW alignment and density.

The alignment process of Ag NWs is shown in Figure 4. Initially, the NWs were roughly aligned on a strained PDMS substrate ( $\epsilon_{\text{pre}} = 80\%$ ) by contact-line deposition<sup>35</sup> (Figure 4a). NWs are considered to be aligned if the skew angle is less than  $5^\circ$  with respect to the transverse direction; 29% of Ag NWs were aligned in this initial step (similar to the reported one-step contact-line deposition).<sup>35</sup> After the strain on the PDMS substrate was released, the alignment of NWs was improved to 56% and the NW density was increased by  $33 \pm 5\%$  (theoretical value:  $(1.8)^{1/2} - 1 = 34\%$ ) (Figure 4b). Figure 4c shows the NWs after they were transferred to the second PDMS substrate (also with a strain of 80%). By comparing Figure 4 panels b and c, we determined that 92% of the Ag NWs were transferred to the second PDMS substrate. The orientation of the NWs on the second substrate is the mirror image of those on the first. Releasing the second PDMS yielded a NW alignment of 90% NWs (Figure 4d). Meanwhile, the NW density increased by  $60 \pm 10\%$  (theoretical value:  $\lambda_1 \lambda_2 \xi - 1 = (1.8)^{1/2} \times (1.8)^{1/2} \times$

$92\% - 1 = 66\%$ , where  $\lambda_1$  and  $\lambda_2$  are the respective stretches in two PDMS substrates and  $\xi$  is the transfer rate of NWs from the first to the second PDMS) after the second transfer/release step, compared to the NW density before the first strain release. To account for the inhomogeneous distribution of NWs, five images of different locations were used to count the number of NWs per unit area before and after release of the PDMS substrate.

Figure 5a shows an optical image of the Si NWs transferred to a strained PDMS substrate using the contact printing method.<sup>19,20</sup> Only a small percentage (25%) of NWs were straight and aligned initially, which was typically the case in our work when contact printing was used for the initial alignment step. Most others were either skewed with respect to the transverse direction or buckled (likely caused by the kinetic friction force during the sliding process). The alignment was improved to 53% and 88%, respectively, after the first release and second transfer/release; 99% of the Si NWs were transferred from the first to the second PDMS substrate. The NW density was increased by  $33 \pm 3\%$  (theoretical value: 34%) and  $75 \pm 7\%$  (theoretical value:  $1.8 \times 99\% - 1 = 78\%$ ), respectively, after the first and second transfer/release step.

The initial step using the contact printing method<sup>19</sup> yielded a degree of alignment less than that which was previously reported. Possible reasons for this include (1) the substrate used here is PDMS instead of silicon or a different plastic.<sup>19</sup> As the NW-substrate interaction (adhesion and friction) plays an important role in the NW alignment,<sup>22</sup> the different interaction with the soft PDMS substrate could be responsible for the poor alignment.<sup>18</sup> (2) Some parameters in the contact printing, such as the contact pressure and sliding force, might have not been optimized. (3) A lubricant, which was found to improve the alignment considerably in previous work,<sup>19</sup> was not used in our process. Nevertheless, even though we did not optimize the contact printing process, we could apply strain-release assembly

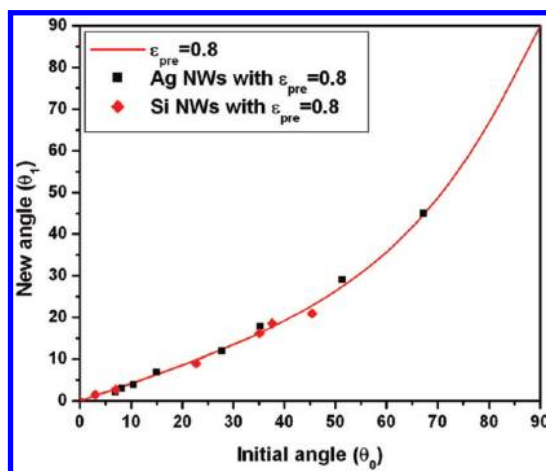


Figure 6. Analytical and experimental results relating the new skew angle to the initial skew angle after release of a strain of 80% in PDMS. The analytical result is from the nonlinear elastic analysis.

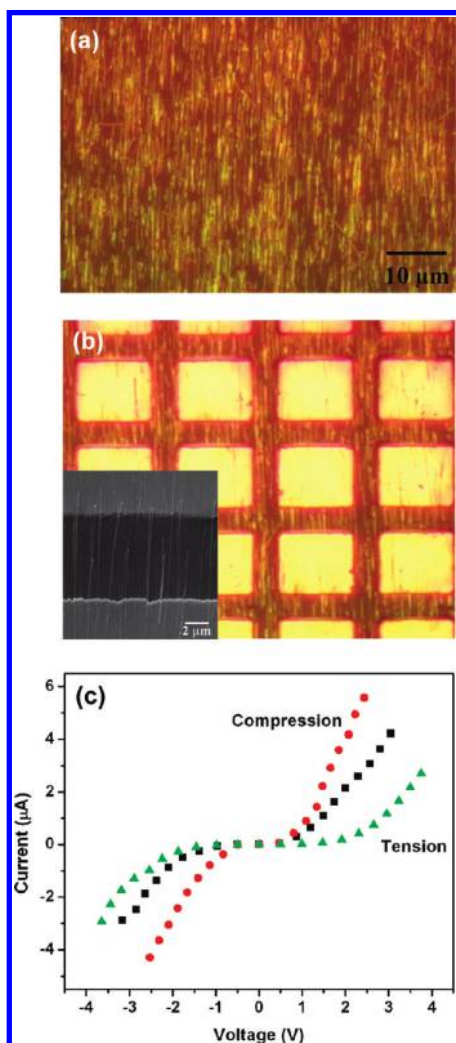


Figure 7. Optical images of the Si NW array (a) before and (b) after the electrode deposition. Inset shows an SEM image of the Si NWs between two metal electrodes. (c)  $I$ - $V$  curve of a NW device as a function of the applied strain ( $\pm 3\%$ ).

to improve the alignment of the NWs. Additionally, when the initial step resulted in a good degree of NW

alignment, the present method can further improve the alignment quality, for example, as shown in Figure 7a.

The new skew angles from a number of Ag and Si NWs after the release of a strain of 80% were measured and plotted in Figure 6 together with the nonlinear elastic analysis. It is seen that the nonlinear elastic predictions agreed with the experimental results remarkably well. Referring to Figure 2b, the linear elastic analysis overestimated the degree of NW alignment.

A two-terminal piezoresistive sensor array was fabricated using the aligned Si NWs on a PDMS substrate to demonstrate how the strain-release assembly technique can be incorporated into a fabrication process to produce a functional device. Thin layers of Ni (20 nm)/Au (80 nm) were evaporated through a shadow mask onto the aligned NWs to serve as electrodes. To improve the electric contact, the devices on PDMS were annealed at 280 °C for 3 min.<sup>39,40</sup> Figure 7 panels a and b show the optical images of the Si NWs before and after the electrode deposition, respectively. Owing to their high-degree of alignment, a large percentage of the NWs bridged the 6  $\mu\text{m}$  gap between the electrodes, even though the length of the NWs was only  $\sim 40\%$  greater than the gap.

Tensile and compressive strains were applied to the PDMS in the direction parallel to the aligned NWs by the Fullam mechanical testing stage loaded in a probe station (Micromanipulator). The current-voltage ( $I$ - $V$ ) response of a Si NW device was measured simultaneously using tungsten probe tips. Figure 7c shows the  $I$ - $V$  response as a function of the applied strain, indicating that the conductance of the Si NWs decreases under tension and increases under compression. The sensing principle is based on the piezoresistivity of Si.<sup>41</sup> Our measured response is similar to the that of Si NW-based strain sensors reported previously,<sup>42,43</sup> but the density of our working devices is orders of magnitude higher than those reported.<sup>42,43</sup>

Importantly, the conductance of the Si NWs returned to its original value once the applied strain (up to  $\pm 3\%$ ) was released, confirming the robustness of the NW devices. The high-degree of alignment and high density of NWs on the substrate guaranteed that nearly every electrode was connected to neighboring electrodes by multiple NWs, ensuring that this process produced a high yield (95%) of working devices. Here we define working devices as those with repeatable, measurable  $I$ – $V$  response within the strain of  $\pm 3\%$ . A common challenge of NW devices on polymer substrates is the contact between the NW and the evaporated electrodes; the contact resistance can change under stretching or bending.<sup>6,7,42,43</sup> Indeed, if a tensile or compressive strain greater than 3% was applied to the sensors, the  $I$ – $V$  curve did not return to its original state, likely due to change in the contact resistance at the NW-electrode interface.

## CONCLUSIONS

We have demonstrated strain-release as a simple yet effective strategy for production of aligned NWs on stretchable substrates. This method can be applied to

NWs synthesized by different methods or processed in different conditions (e.g., wet or dry methods). For instance, the alignment of Ag and Si NWs on PDMS substrates increased from less than 30% to  $\sim 90\%$ , and the density increased by 60–75%, after two assembly steps when the substrates were relaxed from a strain of 80%. The success of this method relies on the large-strain elasticity of the substrates and the static friction between the NWs and the substrate. This method, combined with other alignment techniques, can be applied to a wide variety of nanostructures,<sup>44–46</sup> and the aligned nanostructures can be transferred to other rigid or flexible substrates with the PDMS as a stamp to fabricate multilayered NW devices.<sup>47,48</sup> The highly aligned NWs were instrumental in producing a strain-sensor array with a device yield of 95%. This assembly method can be integrated in the fabrication of NW-based flexible devices (e.g., biosensors and thin-film solar cells), stretchable devices,<sup>9</sup> transparent electronics and electrodes for organic electronics. Furthermore, the fundamental mechanics learned from this work might provide valuable guidelines for other applications involving NW/substrate interfaces.

## METHODS

**Preparation of NWs and PDMS.** Ag NW ink was prepared following the procedure developed by Wiley *et al.*<sup>33</sup> The obtained solution is then diluted in water with the ratio of 1:10 in volume. Boron-doped (p-type) Si NWs were synthesized on Si substrates by chemical vapor deposition (CVD) using gold nanoclusters as catalysts and silane (SiH<sub>4</sub>) as a vapor-phase reactant, following the method reported by Wu *et al.*<sup>34</sup> PDMS substrates with thickness of 2 mm were prepared using “Sylgard 184” (Dow Corning) by mixing the “base” and the “curing agent” with a ratio of 10:1. The mixture was first placed in a vacuum oven to remove air bubbles and then thermally cured at 65 °C for 12 h. Rectangular slabs of suitable sizes were cut from the cured piece.

**Acknowledgment.** This work was supported by the National Science Foundation under Award No. CMMI-1030637. Y.Z. would like to thank W. Fung and Professor W. Lu at the University of Michigan and T. Zhang at Duke University for providing the NW samples.

**Supporting Information Available:** Alignment experiments at the microscale. This material is available free of charge via the Internet at <http://pubs.acs.org>.

## REFERENCES AND NOTES

- Lieber, C. M.; Wang, Z. L. Functional Nanowires. *MRS Bull.* **2007**, *32*, 99–108.
- Xia, Y. N.; Yang, P. D.; Sun, Y. G.; Wu, Y. Y.; Mayers, B.; Gates, B.; Yin, Y. D.; Kim, F.; Yan, Y. Q. One-Dimensional Nanostructures: Synthesis, Characterization, and Applications. *Adv. Mater.* **2003**, *15*, 353–389.
- Lu, W.; Lieber, C. M. Semiconductor Nanowires. *J. Phys. D: Appl. Phys.* **2006**, *39*, R387–R406.
- Duan, X. F. Assembled Semiconductor Nanowire Thin Films for High-Performance Flexible Macroelectronics. *MRS Bull.* **2007**, *32*, 134–141.
- Ju, S. Y.; Facchetti, A.; Xuan, Y.; Liu, J.; Ishikawa, F.; Ye, P. D.; Zhou, C. W.; Marks, T. J.; Janes, D. B. Fabrication of Fully Transparent Nanowire Transistors for Transparent and Flexible Electronics. *Nat. Nanotechnol.* **2007**, *2*, 378–384.
- Lee, J. Y.; Connor, S. T.; Cui, Y.; Peumans, P. Solution-Processed Metal Nanowire Mesh Transparent Electrodes. *Nano Lett.* **2008**, *8*, 689–692.
- McAlpine, M. C.; Friedman, R. S.; Jin, S.; Lin, K. H.; Wang, W. U.; Lieber, C. M. High-Performance Nanowire Electronics and Photonics on Glass and Plastic Substrates. *Nano Lett.* **2003**, *3*, 1531–1535.
- Rathmell, A. R.; Bergin, S. M.; Hua, Y. L.; Li, Z. Y.; Wiley, B. J. The Growth Mechanism of Copper Nanowires and Their Properties in Flexible, Transparent Conducting Films. *Adv. Mater.* **2010**, *22*, 3558–3563.
- Xu, F.; Lu, W.; Zhu, Y. Controlled 3D Buckling of Silicon Nanowires for Stretchable Electronics. *ACS Nano* **2011**, *5*, 672–678.
- Smith, P. A.; Nordquist, C. D.; Jackson, T. N.; Mayer, T. S.; Martin, B. R.; Mbindyo, J.; Mallouk, T. E. Electric-Field Assisted Assembly and Alignment of Metallic Nanowires. *Appl. Phys. Lett.* **2000**, *77*, 1399–1401.
- Chen, X. Q.; Saito, T.; Yamada, H.; Matsushige, K. Aligning Single-Wall Carbon Nanotubes with an Alternating-Current Electric Field. *Appl. Phys. Lett.* **2001**, *78*, 3714.
- Tao, A.; Kim, F.; Hess, C.; Goldberger, J.; He, R. R.; Sun, Y. G.; Xia, Y. N.; Yang, P. D. Langmuir–Blodgett Silver Nanowire Monolayers for Molecular Sensing Using Surface-Enhanced Raman Spectroscopy. *Nano Lett.* **2003**, *3*, 1229–1233.
- Whang, D.; Jin, S.; Wu, Y.; Lieber, C. M. Large-Scale Hierarchical Organization of Nanowire Arrays for Integrated Nanosystems. *Nano Lett.* **2003**, *3*, 1255–1259.
- Messer, B.; Song, J. H.; Yang, P. D. Microchannel Networks for Nanowire Patterning. *J. Am. Chem. Soc.* **2000**, *122*, 10232–10233.
- Huang, Y.; Duan, X. F.; Wei, Q. Q.; Lieber, C. M. Directed Assembly of One-Dimensional Nanostructures into Functional Networks. *Science* **2001**, *291*, 630–633.

16. Yu, G. H.; Cao, A. Y.; Lieber, C. M. Large-Area Blown Bubble Films of Aligned Nanowires and Carbon Nanotubes. *Nat. Nanotechnol.* **2007**, *2*, 372–377.
17. Yu, G. H.; Li, X. L.; Lieber, C. M.; Cao, A. Y. Nanomaterial-Incorporated Blown Bubble Films for Large-Area, Aligned Nanostructures. *J. Mater. Chem.* **2008**, *18*, 728–734.
18. Pevzner, A.; Engel, Y.; Elnathan, R.; Ducobni, T.; Ben-Ishai, M.; Reddy, K.; Shpaisman, N.; Tsukernik, A.; Oksman, M.; Patolsky, F. Knocking Down Highly-Ordered Large-Scale Nanowire Arrays. *Nano Lett.* **2010**, *10*, 1202–1208.
19. Javey, A.; Nam, S.; Friedman, R. S.; Yan, H.; Lieber, C. M. Layer-by-Layer Assembly of Nanowires for Three-Dimensional, Multifunctional Electronics. *Nano Lett.* **2007**, *7*, 773–777.
20. Fan, Z. Y.; Ho, J. C.; Jacobson, Z. A.; Razavi, H.; Javey, A. Large-Scale, Heterogeneous Integration of Nanowire Arrays for Image Sensor Circuitry. *Proc. Natl. Acad. Sci. U.S.A.* **2008**, *105*, 11066–11070.
21. Yerushalmi, R.; Jacobson, Z. A.; Ho, J. C.; Fan, Z.; Javey, A. Large Scale, Highly Ordered Assembly of Nanowire Parallel Arrays by Differential Roll Printing. *Appl. Phys. Lett.* **2007**, *91*, 203104.
22. Fan, Z. Y.; Ho, J. C.; Takahashi, T.; Yerushalmi, R.; Takei, K.; Ford, A. C.; Chueh, Y. L.; Javey, A. Toward the Development of Printable Nanowire Electronics and Sensors. *Adv. Mater.* **2009**, *21*, 3730–3743.
23. Ward, I. M., *Mechanical Properties of Solid Polymers*, 2nd ed.; John Wiley & Sons: Chichester, UK, 1983.
24. Kubo, M.; Li, X.; Kim, C.; Hashimoto, M.; Wiley, B. J.; Ham, D.; Whitesides, G. M. Stretchable Microfluidic Radio Frequency Antennas. *Adv. Mater.* **2010**, *22*, 2749–2752.
25. Zhu, Y.; Xu, F.; Qin, Q. Q.; Fung, W. Y.; Lu, W. Mechanical Properties of Vapor–Liquid–Solid Synthesized Silicon Nanowires. *Nano Lett.* **2009**, *9*, 3934–3939.
26. Bordag, M.; Ribayrol, A.; Conache, G.; Froberg, L. E.; Gray, S.; Samuelson, L.; Montelius, L.; Pettersson, H. Shear Stress Measurements on InAs Nanowires by AFM Manipulation. *Small* **2007**, *3*, 1398–1401.
27. Conache, G.; Gray, S. M.; Ribayrol, A.; Froberg, L. E.; Samuelson, L.; Pettersson, H.; Montelius, L. Friction Measurements of InAs Nanowires on Silicon Nitride by AFM Manipulation. *Small* **2009**, *5*, 203–207.
28. Meyer, E.; Overney, R.; Brodbeck, D.; Howald, L.; Luthi, R.; Frommer, J.; Guntherodt, H. J. Friction and Wear of Langmuir–Blodgett-Films Observed by Friction Force Microscopy. *Phys. Rev. Lett.* **1992**, *69*, 1777–1780.
29. Luthi, R.; Meyer, E.; Haefke, H.; Howald, L.; Gutmannsbauer, W.; Guntherodt, H. J. Sled-Type Motion on the Nanometer-Scale-Determination of Dissipation and Cohesive Energies of C-60. *Science* **1994**, *266*, 1979–1981.
30. Sheehan, P. E.; Lieber, C. M. Nanotribology and Nanofabrication of MoO<sub>3</sub> Structures by Atomic Force Microscopy. *Science* **1996**, *272*, 1158–1161.
31. Qin, Q. Q.; Zhu, Y. Static Friction of Silicon Nanowires on Poly(dimethylsiloxane) Substrates. *Small* **2010** submitted.
32. Lyons, D. M.; Ryan, K. M.; Morris, M. A.; Holmes, J. D. Tailoring the Optical Properties of Silicon Nanowire Arrays through Strain. *Nano Lett.* **2002**, *2*, 811–816.
33. Wiley, B.; Sun, Y.; Mayers, B.; Xia, Y. Shape-Controlled Synthesis of Metal Nanostructures: The Case of Silver. *Chem.—Eur. J.* **2005**, *11*, 454–463.
34. Wu, Y.; Cui, Y.; Huynh, L.; Barrelet, C. J.; Bell, D. C.; Lieber, C. M. Controlled Growth and Structures of Molecular-Scale Silicon Nanowires. *Nano Lett.* **2004**, *4*, 433–436.
35. Deegan, R. D.; Bakajin, O.; Dupont, T. F.; Huber, G.; Nagel, S. R.; Witten, T. A. Capillary Flow as the Cause of Ring Stains from Dried Liquid Drops. *Nature* **1997**, *389*, 827–829.
36. Efimenko, K.; Wallace, W. E.; Genzer, J. Surface Modification of Sylgard-184 Poly(dimethyl siloxane) Networks by Ultraviolet and Ultraviolet/Ozone Treatment. *J. Colloid Interface Sci.* **2002**, *254*, 306–315.
37. Ouyang, M.; Yuan, C.; Muisener, R. J.; Boulares, A.; Koberstein, J. T. Conversion of Some Siloxane Polymers to Silicon Oxide by UV/Ozone Photochemical Processes. *Chem. Mater.* **2000**, *12*, 1591–1596.
38. Song, J.; Tranchida, D.; Vancso, G. J. Contact Mechanics of UV/Ozone-Treated PDMS by AFM and JKR Testing: Mechanical Performance from Nano- to Micrometer Length Scales. *Macromolecules* **2008**, *41*, 6757–6762.
39. Cui, Y.; Zhong, Z. H.; Wang, D. L.; Wang, W. U.; Lieber, C. M. High Performance Silicon Nanowire Field Effect Transistors. *Nano Lett.* **2003**, *3*, 149–152.
40. Zheng, G. F.; Lu, W.; Jin, S.; Lieber, C. M. Synthesis and Fabrication of High-Performance n-Type Silicon Nanowire Transistors. *Adv. Mater.* **2004**, *16*, 1890–1893.
41. He, R. R.; Yang, P. D. Giant Piezoresistance Effect in Silicon Nanowires. *Nat. Nanotechnol.* **2006**, *1*, 42–46.
42. Ryu, S. Y.; Xiao, J. L.; Il Park, W.; Son, K. S.; Huang, Y. Y.; Paik, U.; Rogers, J. A. Lateral Buckling Mechanics in Silicon Nanowires on Elastomeric Substrates. *Nano Lett.* **2009**, *9*, 3214–3219.
43. Lee, C. H.; Kim, D. R.; Zheng, X. L. Fabricating Nanowire Devices on Diverse Substrates by Simple Transfer-Printing Methods. *Proc. Natl. Acad. Sci. U.S.A.* **2010**, *107*, 9950–9955.
44. Engel, M.; Small, J. P.; Steiner, M.; Freitag, M.; Green, A. A.; Hersam, M. C.; Avouris, P. Thin Film Nanotube Transistors Based on Self-Assembled, Aligned, Semiconducting Carbon Nanotube Arrays. *ACS Nano* **2008**, *2*, 2445–2452.
45. Masarapu, C.; Zeng, H. F.; Hung, K. H.; Wei, B. Q. Effect of Temperature on the Capacitance of Carbon Nanotube Supercapacitors. *ACS Nano* **2009**, *3*, 2199–2206.
46. Roberts, M. E.; LeMieux, M. C.; Bao, Z. N. Sorted and Aligned Single-Walled Carbon Nanotube Networks for Transistor-Based Aqueous Chemical Sensors. *ACS Nano* **2009**, *3*, 3287–3293.
47. Feng, X.; Meitl, M. A.; Bowen, A. M.; Huang, Y.; Nuzzo, R. G.; Rogers, J. A. Competing Fracture in Kinetically Controlled Transfer Printing. *Langmuir* **2007**, *23*, 12555–12560.
48. Sun, Y. G.; Rogers, J. A. Fabricating Semiconductor Nano/Microwires and Transfer Printing Ordered Arrays of Them onto Plastic Substrates. *Nano Lett.* **2004**, *4*, 1953–1959.

# Strain-release assembly of nanowires on stretchable substrates

Feng Xu, John W. Durham III, Benjamin J. Wiley and Yong Zhu\*

## SUPPORTING INFORMATION PARAGRAPH

### Alignment experiments at the microscale

Experiments at the microscale were carried out to observe the NW motion in real time during the release of a strained PDMS, as shown in Figure 1S. The PDMS was first scratched slightly by a needle to form an orthogonal pattern to be used as a position reference. A tungsten (W) microrod was selected with  $wL_0/A$  comparable to a typical NW according to Eq. (3). The W microrod has a circular cross-section with diameter of 60  $\mu\text{m}$  and a length of 1mm. The interaction between W and PDMS is van der Waals force. The W microrod was placed on a stretched PDMS with a strain of 60%; see Figure 1Sa. The initial skew angle was measured to be 15.6°. After the strain was released, the new skew angle decreased to 7.1° (Figure 1Sb). Following the real-time observation of the strain release, it is concluded that the microrod rotated simultaneously to adapt to the deformation of the PDMS and slid in the axial direction. The length of the W microrod did not change within the resolution of the optical images (half pixel, equivalent to 50 nm). The new skew angle is plotted in Figure 1Sc as a function of the applied strain and the initial skew angle. The real-time experiments at the microscale corroborated the NW experiments and the nonlinear elastic analysis.

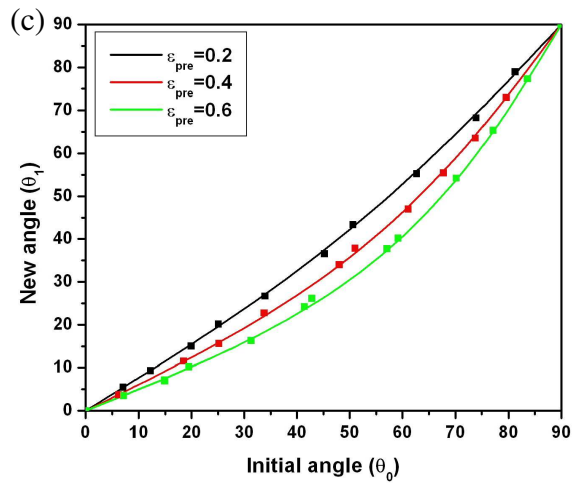
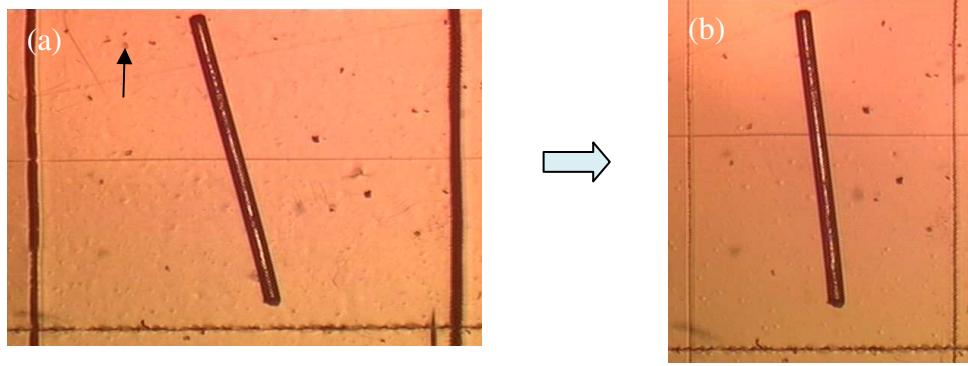


Figure 1S. Optical images showing a W microrod on the PDMS (a) before and (b) after the strain (60%) was released. The dots pointed by the arrow in (a) were out of the view in (b), indicating that the microrod slid during the strain release. (c) The new skew angle as a function of the initial skew angle under strains of 20%, 40% and 60%. The lines represent the analytical results from the nonlinear elastic model and the dots represent the experimental results.